Opt Rev (2015) 22:553–559
DOI 10.1007/s10043-015-0094-5

REGULAR PAPER

All-optical pulsewidth-tunable wavelength conversion of return-to-zero differential phase-shift keying signal

Gazi Mohammad Sharif[1] · Quang Nguyen-The[2] · Motoharu Matsuura[1] · Naoto Kishi[1]

Received: 3 February 2015 / Accepted: 2 May 2015 / Published online: 22 May 2015

Abstract We demonstrate the wavelength conversion of return-to-zero differential phase-shift keying (RZ-DPSK) signal with the pulsewidth-tunable operation using a Raman amplifier (RA)-based ultrashort pulse compressor and a highly nonlinear fiber (HNLF)-based four-wave mixing (FWM) switch. The wavelength of the input RZ-DPSK signal is converted to new wavelengths owing to the FWM effect in HNLF. On the other hand, the pulsewidth of the wavelength-converted RZ-DPSK signal is tuned from 10 to 3 ps by using the ultrashort pulse source based on RA-based adiabatic soliton pulse compression. The bit error rate characteristics of the input RZ-DPSK and the wavelength-converted RZ-DPSK signals with different pulsewidths are measured and error-free operations are achieved in all cases. The optical spectra, autocorrelation traces, and clear and opening eye diagrams show high conversion performance with wide-range pulsewidth tunability.

Keywords RZ-DPSK · Wavelength conversion · Pulsewidth-tunable operation · Raman amplifier · Four-wave mixing (FWM)

✉ Gazi Mohammad Sharif
gazi.md.sharif@uec.ac.jp

[1] Department of Communication Engineering and Informatics, The University of Electro-Communications, Tokyo 182-8585, Japan

[2] Faculty of Radio-Electronics, Le Quy Don Technical University, Hanoi, Vietnam

1 Introduction

Wavelength conversion is an important technique for future wavelength-division multiplexing (WDM) systems to optimize the network performance by avoiding the network congestion without employing further network paths or packet buffering [1, 2]. On the other hand, nowadays, the differential phase-shift keying (DPSK) format is considered as a promising modulation format for future photonic networks owing to its 3-dB higher receiver sensitivity than that of on–off keying (OOK) format [3]. Because of the higher receiver sensitivity and nonlinear tolerance compared with OOK format, recently the DPSK format receives great attentions for future high-speed photonic networks [4, 5]. In particular, return-to-zero (RZ)-DPSK signal is considered as a promising technique for its superior performances in optical transmission systems [6]. Thus, wavelength conversion of RZ-DPSK signal seems interesting owing to its great influences for implementing in future high-speed photonic systems and has been demonstrated in some literatures [7–9]. Among some techniques for wavelength conversion, four-wave mixing (FWM) process is considered as a very useful technique because of its advantages such as bitrate and modulation format transparency [10] and elimination of optical–electrical–optical (O–E–O) conversion. Moreover, the signal degradation is negligible in FWM due to the little noise or chirping effect. The employed optical filters for suppressing the unwanted optical signals are low cost, low loss and well matched with the standard transmitting fiber [11]. Thus, FWM is suitable for both OOK and phase-modulated signals for the wavelength conversion [12]. Efficient wavelength conversion using FWM needs a pump signal with high power for energy transfer to the idler waves during propagating with a probe signal in a highly

nonlinear optical media. For the FWM effect, the converted signals at frequencies $2\omega_p$ - ω_s and $2\omega_s$ - ω_p are generated, where ω_p and ω_s are pump and probe frequencies, respectively. Usually, the continuous waves (CWs) are used as pumps for wavelength conversion of signals [8, 9] for the simplicity avoiding the extra modulators. However, wavelength conversion for RZ-DPSK signal has also been demonstrated in some works, where the RZ pulse trains were employed as pumps [13, 14]. The advantages of pulse train over CW have been mentioned in these works such as the spectrum of the pulse train is broader than that of CW and it is potential for 3R generation (reamplifying, reshaping, and retiming) [13]. Another great advantage of pulse train over CW is that, phase modulation to suppress the stimulated Brillouin scattering effect [13, 15] is not necessary. Thus, RZ pulse trains are more effective than CW pumps for these reasons. On the other hand, the pulsewidth of a signal plays very important roles owing to its influences on some features such as dispersion and nonlinearity tolerances. These effects degrade the signal qualities and need changes of the systems to eliminate the problems. However, changing the parameters of existing infrastructure is not feasible. Hence, to solve the problems, the solution may be the tunability and flexibility with the existing systems for variable situations. The concept of changing the pulsewidth has come based on it to optimize the transmission systems for different situations, hence pulsewidth tunability without intersymbol interference between the neighboring pulses is essential [16, 17]. In addition, the optimum pulsewidth of OTDM systems is determined by its bitrate. Thus, the pulsewidth for the OTDM systems should be tuned in a wider operating range for applying to OTDM systems with the arbitrary bitrate. Moreover, very short pulsewidth is needed for high-speed OTDM systems to avoid the cross talks between the channels. It was mentioned earlier that wavelength conversion of RZ-DPSK signal has already been demonstrated in some works. However, the pulsewidth tunability of the wavelength-converted RZ-DPSK signal was not considered in these experiments.

In this study, we investigate the characteristics of wavelength conversion of RZ-DPSK signal for the first time, where the pulsewidth of the converted signal is tuned in a wider range. The wavelength conversion is achieved with the FWM effect in highly nonlinear fiber (HNLF) and the pulsewidth-tunable operation is demonstrated using a Raman amplifier (RA)-based pulse compressor. In our experiment, an RZ clock was employed as a pump signal for the wavelength conversion with pulsewidth-tunable operation. By changing the Raman pump power of the RA-based pulse compressor, the pulsewidth of the compressed pump signal is tuned, which leads to the pulsewidth tunability of the wavelength-converted signal from 10 to 3 ps. The pulse pedestals [18] produced in pulse compressor are eliminated owing to the input–output characteristics of FWM process of the wavelength converter [19]. The pedestal-free waveforms are very important for high bitrate OTDM systems to avoid the bit overlapping between the neighboring pulses. Moreover, the measured traces of the waveforms are well fitted by sech^2 fitting, the obtained optical spectra, eye diagrams, and the bit error rate (BER) characteristics show good quality wavelength conversion with wide-range pulsewidth tunability.

2 Operation principle and experimental setup

The schematic diagram of the wavelength converter is shown in Fig. 1. It consists of an RA-based pulse compressor and a fiber-based FWM switch. The switch also acts as an AND gate. The pulsewidth of the RZ clock is compressed and tuned in the RA-based pulse compressor. The compressed and duration-tuned RZ clock and the input RZ-DPSK signal are nonlinearly interacted inside the fiber-based FWM switch to produce new wavelength-converted RZ-DPSK signals. In this scheme, the pulsewidth of the wavelength-converted RZ-DPSK signal is tuned owing to the pulsewidth tunability of the RZ clock. Even if pulse pedestals are generated in the compressor, pulse pedestals of the converted signal are eliminated owing to the property of FWM switch [19], as P_{FWM} is proportional to the square of P_{pump}, shown in the following expression [20]:

$$P_{\text{FWM}} = \eta\gamma^2 P^2{}_{\text{pump}} P_{\text{sig}} e^{-\alpha L}\left[\frac{(1-e^{-\alpha L})^2}{\alpha^2}\right], \quad (1)$$

where P_{FWM} is the power of the newly generated FWM signal, η, and γ are the FWM efficiency and the nonlinear coefficient of the fiber, respectively. P_{pump} and P_{sig} denote the powers of the pump and probe signals propagating through HNLF, respectively. α and L are the attenuation coefficient and the length of the fiber, respectively.

The experimental setup of wavelength conversion of RZ-DPSK signal is shown in Fig. 2. Two external-cavity laser diodes (ECL) and an electroabsorption modulator (EAM) were used to generate two 10 GHz RZ clocks at the wavelengths of 1552.52 and 1558.17 nm. These RZ clocks were sech^2 shaped pulses of 20 ps. An erbium-doped fiber amplifier (EDFA) was employed at the output of the RZ clock generator for compensating the insertion loss of the EAM and to adjust the fundamental soliton power for the RA-based pulse compressor. As the soliton power condition is very important for the adiabatic pulse compression method [21], the average power for the input RZ clock was

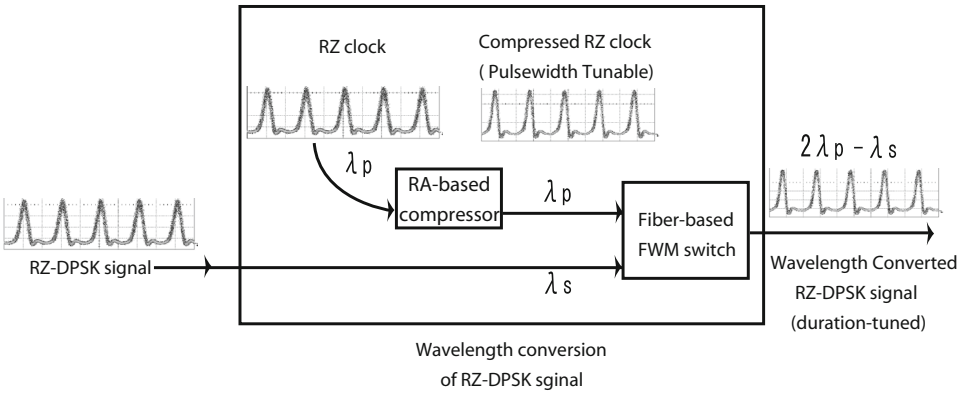

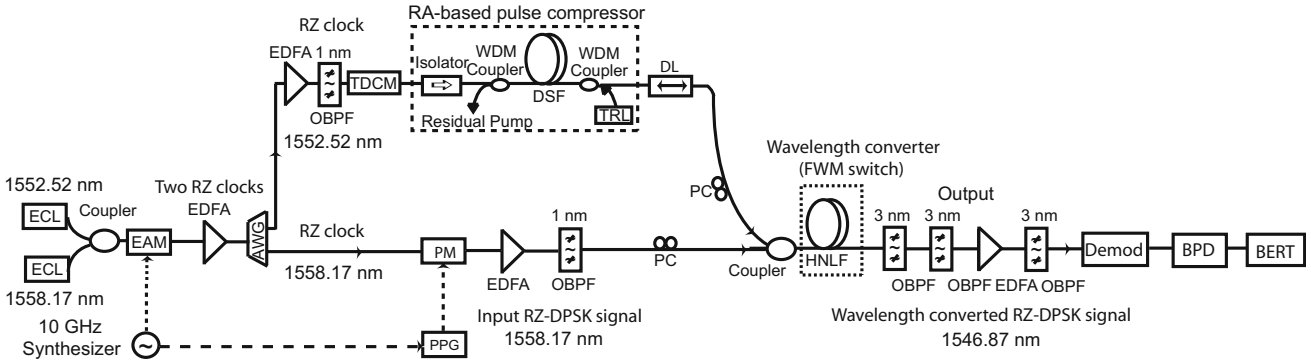

Fig. 1 Scheme of wavelength conversion of RZ-DPSK signal

Fig. 2 Experimental setup for wavelength conversion of RZ-DPSK signal with pulsewidth tunability

calculated using Eq. (2) and was set as 6.2 dBm. The fundamental soliton pulse of sech^2 pulse ($N = 1$) has a peak power [19, 22]:

$$P_1 = \frac{0.777\lambda^3 D A_{\text{eff}}}{\pi^2 c n_2 \tau_{\text{FWHM}}^2}, \tag{2}$$

where P_1 is the peak power of the fundamental soliton pulse. λ, D, c, and n_2 are the wavelength of the optical pulse, the chromatic dispersion ($D > 0$), the speed of light in vacuum, and the nonlinear refractive index, respectively. A_{eff} and τ_{FWHM} are the effective area and the pulse duration of the optical mode, respectively. By rearranging Eq. (2), the relationship between the soliton pulse duration, the peak power of the optical pulse, and chromatic dispersion can be reformulated in Eq. (3):

$$\tau_{\text{FWHM}} \propto \sqrt{\frac{D}{P_1}}, \tag{3}$$

where the square of the soliton pulse duration τ_{FWHM} is proportional to the chromatic dispersion D and inversely proportional to the peak power P_1 of the optical pulse. Therefore, the pulsewidth of the RZ clock can be compressed by either decreasing the dispersion value, which is not possible continuously in real deployment or increasing the Raman pump power since the soliton condition is maintained during the amplification, which is feasible.

An optical band pass filter (OBPF) after the EDFA was used to suppress the out-of-band amplified spontaneous emission (ASE) noise of the EDFA. The following arrayed waveguide grating (AWG) separates the two RZ clocks with their wavelengths. The RZ clock at the wavelength of 1552.52 nm acted as the pump signal since the wavelength was chosen to match the zero-dispersion wavelength of the HNLF for the efficient nonlinear effects. The negative chirp of the RZ clock induced in EAM was suppressed using a tunable dispersion-compensating module (TDCM) before it entered the RA-based pulse compressor and after the TDCM, the pulsewidth of the RZ clock was 17 ps. The pulse compressor includes a 17-km dispersion-shifted fiber (DSF) and a wavelength-tunable Raman laser (TRL) for the Raman pump in the counterpropagating direction using a WDM coupler. The DSF with its characteristics is described in Table 1. To achieve high quality compression, the wavelength of the TRL was tuned to 1452 nm, where the pulsewidth of the compressing RZ clock was 1552.52 nm. Here, the wavelength difference of the Raman pump and RZ clock was about 100 nm, corresponding to the Raman Stoke's shift of 13.2 THz. When the Raman pump power is increased, the pulsewidth of the RZ clock is

Table 1 Characteristics of dispersion-shifted fiber

Parameter	Value	Unit
Length	17	km
Dispersion at 1552 nm	3.8	ps/nm/km
Dispersion slope at 1552 nm	0.059	ps/nm^2/km
Attenuation	0.197	dB/km

compressed owing to the soliton condition maintained in the DSF during amplification [21].

The another RZ clock at a wavelength of 1558.17 nm was used to generate a 10 Gb/s RZ-DPSK signal with a phase modulator (PM) and a pulse pattern generator (PPG). The RZ-DPSK data was encoded by a pseudorandom bit sequence (PRBS) with a pattern length of $2^{31}-1$. The following EDFA was employed to improve the extinction ratio of the input RZ-DPSK signal. The following OBPF was for eliminating the out-of-band ASE noise of the EDFA as the same function of the previous OBPF. The duration-tuned RZ clock and the input RZ-DPSK signal were coupled by a 3-dB coupler before entering to the fiber-based FWM switch. In the FWM switch, a 500-m-long HNLF was used for the wavelength conversion of the input RZ-DPSK signal where the RZ clock was used as a pump. The HNLF with its characteristics is described in Table 2.

The optical delay line (DL) was employed for the time synchronization between the RZ clock and the input RZ-DPSK signal for the efficient FWM effect. The polarization controllers (PCs) were employed to set the related states of polarization of the pump and data signals. The wavelength-converted RZ-DPSK signal at the wavelength of 1546.87 nm was filtered by two cascaded OBPFs and then amplified by an EDFA with another OBPF. Then, the signal is injected into the demodulator (Demod) and the balanced photodiode (BPD). The BER tester (BERT) is employed to measure the BER characteristics of the wavelength-converted RZ-DPSK signal.

Table 2 Characteristics of highly nonlinear fiber (HNLF)

Parameter	Value	Unit
Length	500	m
Dispersion at 1552 nm	−0.08	ps/nm/km
Dispersion slope at 1552 nm	0.032	ps/nm^2/km
Attenuation	0.47	dB/km
Nonlinear coefficient (γ)	12.6	W^{-1} km^{-1}
Affective area (A_{eff})	11	μm^2

3 Experimental results and discussion

Figure 3 shows the FWM spectra of for the case of the wavelength-converted signal with 3 ps pulsewidth. The signal at the wavelength of 1546.87 nm was generated from the input RZ-DPSK signal at the wavelength of 1558.17 nm owing to the FWM effect induced by the RZ clock at the wavelength of 1552.52 nm. In our experiment, the top power level difference between the input and conjugated signal of the HNLF output spectrum, hence the FWM efficiency, was −18 dB.

By changing the Raman pump power from 0.48 to 0.85 W, the controlled pulsewidth of the wavelength-converted RZ-DPSK signal was tuned continuously from 10 to 3 ps as a function of Raman pump power as shown in Fig. 4. It should be mentioned that, the waveform was severely distorted when Raman pump power was larger than 1 W owing to the fluctuation from the adiabatic condition inside the compressor [18]. An autocorrelator was employed to observe the quality and the accurate short pulsewidth of the converted signal. The autocorrelation traces of the wavelength-converted signals with 10 and 3 ps are shown in Fig. 5. For both cases, the pulse waveforms were well matched and fitted by sech^2 and the pulse pedestal components [18] were suppressed owing to the input–output features of FWM process [19]. The quadratic dependence of the converted RZ-DPSK data on the power of the pump is shown in Eq. (1). The pedestal-free short pulsewidths are very important for OTDM systems to avoid the bit overlapping between the neighboring pulses in OTDM systems.

The wavelength-converted RZ-DPSK signal with various pulsewidths was measured with a 30-GHz-bandwidth sampling oscilloscope. The eye diagrams of the

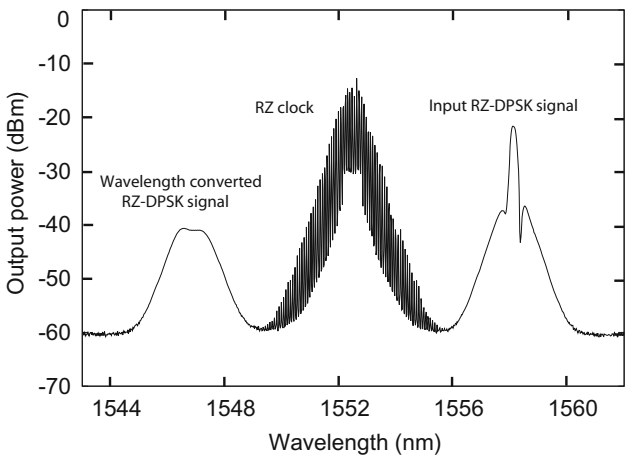

Fig. 3 FWM spectrum of input RZ-DPSK and wavelength-converted RZ-DPSK signals

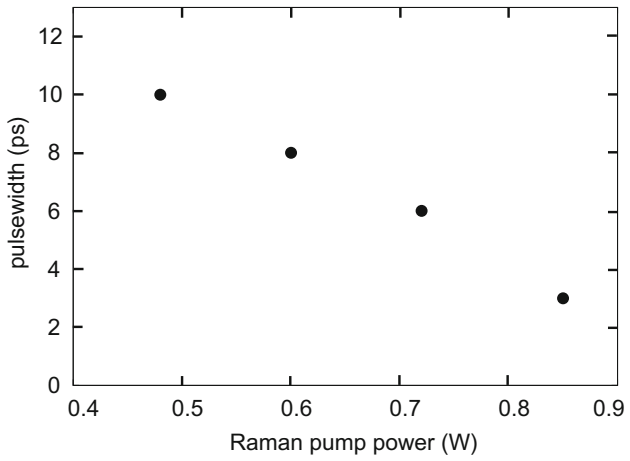

Fig. 4 Raman pump power dependency of the wavelength-converted RZ-DPSK signal with various controlled pulsewidths

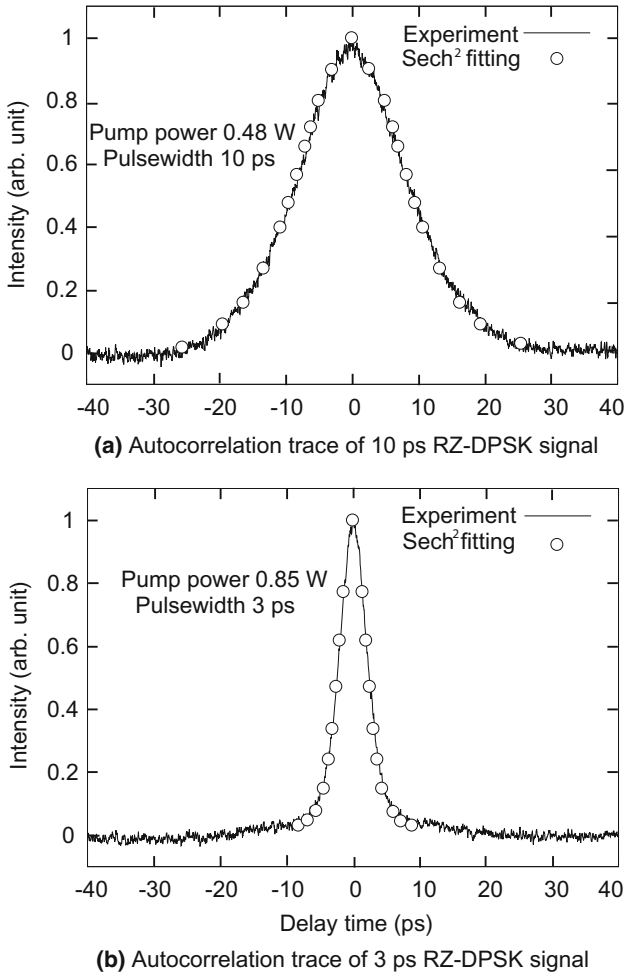

Fig. 5 Autocorrelation traces of wavelength-converted RZ-DPSK signals

wavelength-converted modulated and demodulated RZ-DPSK signals with 10 and 3 ps pulsewidths are shown in Fig. 6. The actual pulsewidths of the signal could not be estimated owing to the limited bandwidth of the oscilloscope with 30 GHz. However, for both converted modulated and demodulated signals, clear and opening eye diagrams were observed. The demodulated pulsewidth was quite wider than the optical pulse owing to the limited bandwidth of BPD with 17 GHz. Moreover, the intersymbol interference or pulse overlap was seen for the converted demodulated 3 ps RZ-DPSK signal. However, the error-free operation was achieved for the converted demodulated 3 ps RZ-DPSK signal. Thus, the performance of this optical pulse might be sufficient in the differential detection system. In our experiment, the error-free operation was not attained for less than 3 ps converted signal.

Figure 7 shows the BER characteristics of the input RZ-DPSK and wavelength-converted RZ-DPSK signals with 10 and 3 ps pulsewidths. Error-free operations were achieved for both 10 and 3 ps wavelength-converted signals with less than 2-dB power penalties compared with the input RZ-DPSK signal at BER $= 10^{-9}$. The power penalties were due to the wavelength conversion process using FWM [23] and the RA-based pulse compression [18]. It was mentioned earlier that when the Raman pump power is more than 1 W, the adiabatic soliton condition is deviated. Therefore, error-free operation with pulsewidth less than 3 ps was not achieved. Almost same BER performance could be obtained for the pulsewidth between 3 and 10 ps. However, in our case, the pulsewidth of 3 ps was slightly worse than the pulsewidth of 10 ps. This might be due to the effect of Raman saturated powers on the signals with short pulsewidths, as the tendency of breaking the soliton condition starts with increasing the Raman pump power.

The role of the RA compressor is not only the pulse compressor but also the amplifier. When the gain is changed, it influences the high conversion performance. The Raman gain was 10 dB for the pulsewidth of 10 ps and 15 dB for the pulsewidth of 3 ps. Here, the gain variation of 5 dB and the noise figure (NF) affect the converted signals.

An ultrashort pulsewidth is needed for high-speed OTDM systems to avoid the cross talks between the channels after multiplexing. Hence, the picosecond pulsewidth is very important for the OTDM systems. As an example, the pulsewidth of a 160 Gbit/s OTDM system is estimated to be less than 2 ps [24]. Since, the input pulse can be tuned to short pulsewidth by changing the Raman pump power, this wavelength converter is applicable for ultrahigh-speed OTDM application.

On the other hand, tunable wavelength conversion in a wider operating range is effective for wavelength routing and switching [25]. Though, in this work, tunable wavelength conversion was not investigated, it can be achieved by proper tuning the wavelength of the RZ

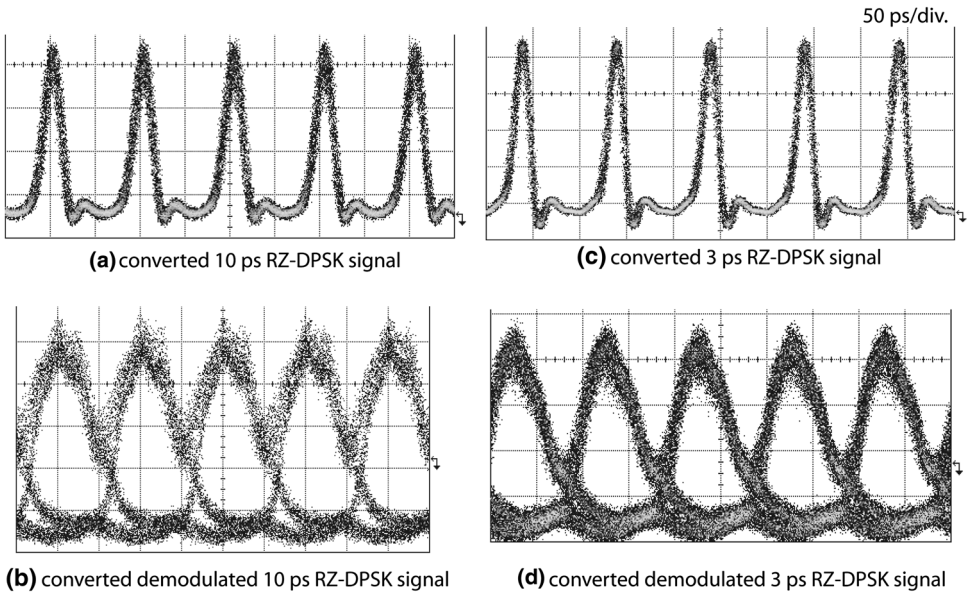

Fig. 6 Eye diagrams of wavelength-converted modulated and demodulated RZ-DPSK signals with the pulsewidths of 10 and 3 ps

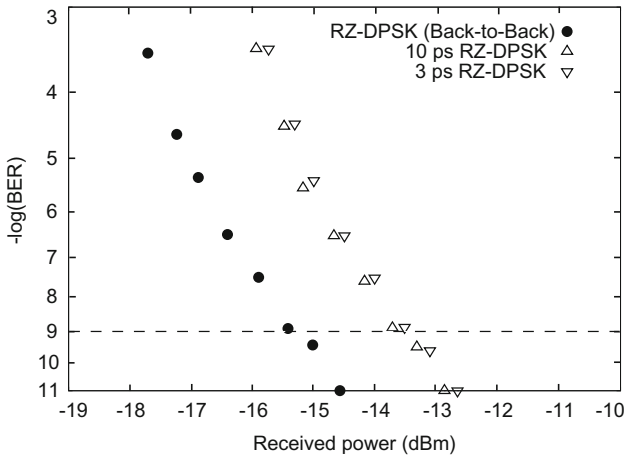

Fig. 7 BER characteristics input RZ-DPSK, and wavelength-converted RZ-DPSK signals with the pulsewidths of 10 and 3 ps

clock. In that case, the wavelength of input RZ-DPSK signal could be fixed as zero-dispersion wavelength and the tunable wavelength conversion can be done by changing the wavelength of the RZ clock in an optimum operating range. It should be noted that the wavelength of the TRL will also be tuned according to the Raman Stoke's shift.

The state of polarization (SOP) fluctuates when the signal travels in installed fiber in real deployment. Therefore, polarization insensitive operation is necessary in transmitting systems [26]. Though our proposed system is polarization sensitive, polarization insensitive operation could be employed by adding extra features like polarization diversity loop [27] inside the converter.

4 Conclusions

We have experimentally demonstrated all-optical wavelength conversion of RZ-DPSK signal with short pulsewidth-tunable operation by the combination of RA-based pulse compressor and fiber-based FWM switch. By adjusting the Raman pump power, the pulsewidth of the wavelength-converted signal can be continuously tuned from 10 to 3 ps. In our scheme, the combination of wavelength conversion and pulsewidth tunability can promote the OTDM technology for the arbitrary bitrates and diverse conditions.

Acknowledgments This work was partly supported by JSPS KAKENHI Grant Number 24360148.

References

1. Yoo, S.J.B.: J. Lightwave Technol. **14**, 955 (1996)
2. Ramamurthy, B., Mukherjee, B.: IEEE J. Sel. Areas Commun. **16**, 1061 (1998)
3. Gnauck, A.H., Winzer, P.J.: J. Lightwave Technol. **23**, 115 (2005)
4. Tonguz, O.K., Wagner, R.E.: IEEE Photonics Technol. Lett. **3**, 835 (1991)
5. Elrefaie, A.F., Wagner, R.E.: IEEE Photonics Technol. Lett. **3**, 71 (1991)
6. Cai, J.-X., Foursa, D.G., Liu, L., Davidson, C.R., Cai, Y., Patterson, W.W., Lucero, A.J., Bakhshi, B., Mohs, G., Corbett, P.C., Gupta, V., Anderson, W., Vaa, M., Domagala, G., Mazurczyk, M., Li, H., Jiang, S., Nissov, M., Pilipetskii, A.N., Bergano, Neal S.: J. Lightwave Technol. **23**, 95 (2005)
7. Li, Z., Dong, Y., Mo, J., wang, Y., Lu, C.: IEEE Photonics Technol. Lett. **16**, 1685 (2004)
8. Matsuura, M., Kishi, N.: IEEE Photonics Technol. Lett. **23**, 615 (2011)

9. Andersen, P.A., Tokle, T., Geng, Y., Peucheret, C., Jeppesen, P.: IEEE Photonics Technol. Lett. **17**, 1908 (2005)
10. D'Ottavi, A., Spano, P., Hunziker, G., Paiella, R., Dall'Ara, R., Guekos, G., Vahala, K.J.: IEEE Photonics Technol. Lett. **10**, 952 (1998)
11. Yu, C., Pan, Z., Wang, Y., Song, Y.W., Gurkan, D., Hauer, M.C., Starodubov, D., Willner, A.E.: IEEE Photonics Technol. Lett. **16**, 1906 (2004)
12. Astar, W., Lenihan, A.S., Carter, G.M.: IEEE Photonics Technol. Lett. **19**, 1676 (2007)
13. Hu, H., Wang, W., Yu, J.: Microw. Opt. Technol. Lett. **54**, 2172 (2012)
14. Geng, Y., Peucheret, C., Jeppesen, P.: Presented at MP5, Laser and Eeletronic Society, (2006)
15. Lu, G.-W., Abedin, K.S., Miyazaki, T., Marhic, M.E.: Electron. Lett. **45**, 221 (2009)
16. Sano, A., Miyamoto, Y., Kataoka, T., Hagimoto, K.: J. Lightwave Technol. **16**, 977 (1998)
17. Yan, L.-S., Nezam, S.M.R.M., Sahin, A.B., McGeehan, J.E., Luo, T., Yu, Q., Willner, A.E.: In: Proceedings of 28th European conference on optical communications, 2002, p. 10.6.2
18. Matsuura, M., Samarakoon, B.P., Kishi, N.: IEEE Photonics Technol. Lett. **21**, 572 (2009)
19. Nguyen-The, Q., Matsuura, M., Tan, H.N., Kishi, N.: IEICE Trans. Electron E94-C 1160 (2011)
20. Bogris, A., Syvridis, D.: J. Lightwave Technol. **21**, 1892 (2003)
21. Reeves-Hall, P.C., Taylor, J.R.: Electron. Lett. **37**, 417 (2001)
22. Agrawal, G.P.: Nonlinear Fiber Optics. Academic Press, New York (1995)
23. Inoue, K., Toba, H.: IEEE Photonics Technol. Lett. **4**, 69 (1992)
24. Weber, H.-G., Nakazawa, M.: Ultrahigh-Speed Optical Transmission Technology. Springer, New York (2010)
25. Pu, M., Hu, H., Galili, M., Ji, H., Peucheret, C., Oxenløwe, L.K., Yvind, K., Jeppesen, P., Hvam, J.M.: IEEE Photonics Technol. Lett. **23**, 1409 (2011)
26. Kwok, C.H., Lin, C.: IEEE J. Sel. Top. Quantum Electron. **12**, 451 (2006)
27. Hasegawa, T., Inoue, K., Oda, K.: IEEE Photonics Technol. Lett. **5**, 947 (1993)